Supporting Information for:

Methanol Dimer Formation Drastically Enhances Hydrogen Abstraction from Methanol by OH at Low Temperature

Willem Siebrand,[†] Zorka Smedarchina,[†] Emilio Martínez-Núñez,[*,‡] and Antonio Fernández-Ramos[*,‡]

National Research Council of Canada, Ottawa, Ontario K1A 0R6, Canada, and Departmento de Química Física e Centro Singular de Investigación en Química Biolóxica e Materiais Moleculares (CIQUS), Universidade de Santiago de Compostela, 15782 Santiago de Compostela, Spain

E-mail: emilio.nunez@usc.es; qf.ramos@usc.es

[*]To whom correspondence should be addressed
[†] National Research Council of Canada
[‡] Universidade de Santiago de Compostela

Index

S1. Electronic structure calculations

S1.1. Adequacy of the MPWB1K/6-31+G(d,p) potential energy surface

Apart from the justifications provided in the manuscript about the adequacy of the MPWB1K/6-31+G(d,p) level of theory, here we provide additional arguments that justify our choice.

We have performed canonical variational transition state theory calculations (CVT) with small-curvature tunneling corrections (SCT) for the hydrogen abstraction reaction at room temperature, because experimental data are available.[1] Large-curvature tunneling (LCT) probabilities were also calculated but the resulting microcanonically optimized tunneling probabilities (the largest between SCT and LCT tunneling probabilities at every tunneling energy) were indistinguishable from the SCT values. At 298 K the experimental value is 9.4×10^{-13} cm^3 molecule^{-1} s^{-1}, whereas our calculated value is 8.9×10^{-13} cm^3 molecule^{-1} s^{-1}. These two values also agree very well with the calculated rate constant reported by Xu and Lin (Ref. 1 of the manuscript) evaluated at the CCSD(T)//MP2/6-311+G(3df,2p) level and with a value of 8.0×10^{-13} cm^3 molecule^{-1} s^{-1}. This is already a good indicator that both methods lead to similar results.

The thermal rate constants measured by SBGH (Ref. 4 of the manuscript) and by Gomez-Martin et al. (Ref. 8 of the manuscript) at low temperatures using a Laval nozzle cannot be simulated by variational transition state theory, but it is still possible to check the accuracy of the electronic structure and dynamics calculations. For this purpose we compare our values to the previous calculations carried out by SBGH. These authors performed master equation calculations using the previous electronic structure information obtained by Xu and Lin, although additionally they fitted barrier heights, the well depth of the complex and the imaginary frequency of the transition states to the observed thermal rate constants above 200 K. Our calculations, which do not involve any empirical fitting, are only twice larger than experiment (and the calculated values of SBGH) at 200 K. As temperature decreases the calculated rate constants by SBGH increase faster than our calculated thermal rate constants and they become larger at temperatures below 100 K. To our understanding this sudden increase of the thermal rate constants at low temperatures is due to an overestimation of the tunneling contribution. It has been shown by some of us in the hydrogen abstraction reaction of methanol by atomic hydrogen[2] that one-dimensional Eckart barriers may lead to potentials which are too narrow, increasing artificially the tunneling probabilities. Because tunneling probabilities are proportional to the value of the imaginary frequency at the transition state, this seems also the case in the work of SBGH, in which the imaginary frequency at the transition state for reaction R2a (the main channel below 100 K) is 2564 cm^{-1}. This value of the imaginary frequency is very high for this type of

reaction and cast some doubts about the adequacy of the MP2/6-311+G(3df,2p) level upon which is based. The MP2 imaginary frequency is even higher, with a value of 2958 cm^{-1}.   In this context the imaginary frequency calculated at the MPWB1K/6-31G(d,p) level is 1737   cm^{-1}, which is a more reasonable value for a hydrogen abstraction reaction. It is worth noting that our tunneling calculations also lead to branching ratios which are in agreement with experiment without assuming unphysical parameters.

As a final test the QCT association rate constant at 50 K obtained from the analytical potential energy surface built using MPWB1K/6-31+G(d,p) calculations is 2.78 $\times10^{-10}$ cm^3 molecule^{-1} s^{-1}, which is very close to the value of 3.0$\times10^{-10}$ cm^3 molecule^{-1} s^{-1} reported by SBGH for the same association reaction.

Therefore, the dynamics calculations for the reaction of the monomer of methanol with OH using the MPWB1K/6-31+G(d,p) level compare well with previous dynamics calculations carried out by SBGH and based on the electronic structure computations of Xu and Lin (plus empirical fitting), in spite of the differences between the two potential energy surfaces. It also becomes clear that the discrepancy between theory and experiment is not due to possible inaccuracies in the potential energy surface and cannot be resolved by assuming that the reaction exclusively takes place between the methanol monomer and the OH radical.

S1.2. MPWB1K/6-31+G(d,p) stationary points

Optimized geometries of the stationary points calculated at the MPWB1K/6-31+G(d,p) level. Cartesian coordinates (in Å), absolute energies (in a.u.) and unscaled frequencies (in cm^{-1}). For the rate constant calculations all frequencies have been scaled by 0.964.

Methanol

Cartesian coordinates:

```
     O          0.000000     0.000000     0.000000
     H          0.000000     0.000000     1.084578
     H          1.035914     0.000000    -0.341755
     H         -0.484488    -0.915645    -0.341734
     O         -0.691828     1.148714    -0.407349
     H         -0.714271     1.185931    -1.359443
```

Absolute energy: -115.666762

Frequencies:

```
    325         1084         1145
   1205         1385         1517
   1533         1545         3086
   3148         3221         4011
```

Hydroxyl radical

Cartesian coordinates:

```
     O          0.000000     0.000000     0.107486
     H          0.000000     0.000000    -0.859886
```

Absolute energy: –75.702715

Frequencies: 3865

Methanol···OH complex

Cartesian coordinates:

```
C       −0.118032   −0.197184   −0.167717
H       −0.564423   −0.961230    0.458132
H        0.964842   −0.258104   −0.072909
H       −0.458498    0.777762    0.176636
O       −0.540158   −0.453352   −1.486222
H       −0.170106    0.188327   −2.086785
O       −1.492003   −2.964257   −2.353011
H       −1.174586   −2.084419   −2.073334
```

Absolute energy: –191.381365

Frequencies:

```
  34        62       203
 319       453       654
1102      1132      1206
1389      1517      1534
1545      3107      3181
3235      3694      4009
```

Methanol dimer

Cartesian coordinates:

```
C        2.259752   −0.350096    0.236745
O        1.269600    0.583267   −0.125066
H        1.881850   −0.892051    1.095958
H        3.188584    0.143422    0.518411
H        2.455391   −1.062531   −0.563202
H        1.557497    1.082844   −0.885037
H       −0.490900   −0.091876   −0.349024
O       −1.369294   −0.443427   −0.517231
C       −2.283072    0.149282    0.355722
H       −3.262914   −0.263292    0.134500
H       −2.055823   −0.063157    1.402743
H       −2.336211    1.232811    0.229229
```

Absolute energy: –231.343243

Frequencies:

```
  23        43        51
 104       123       190
 367       709      1097
1131      1136      1159
1206      1208      1389
1443      1516      1518
1532      1534      1544
1547      3072      3106
3128      3179      3200
3234      3859      4003
```

Methoxy radical

Cartesian coordinates: (in Å) of

```
    C        −0.572038     0.000240    −0.012301
    O         0.785827     0.000101    −0.007620
    H        −0.862486    −0.008986     1.048323
    H        −0.996424     0.906473    −0.449844
    H        −0.995481    −0.899735    −0.463710
```

Absolute energy: −114.997995

Frequencies:

```
   872        992       1176
  1412       1416       1550
  3016       3099       3143
```

Hydroxymethyl radical

Cartesian coordinates:

```
    C         0.070455     0.121928     0.047204
    H        −0.034382    −0.003604     1.110072
    H         1.014860    −0.062948    −0.441762
    O        −0.754653     1.058342    −0.468602
    H        −0.589494     1.172472    −1.401246
```

Absolute energy: −115.006263

Frequencies:

```
   438        619       1075
  1279       1374       1527
  3217       3367       4005
```

Water

Cartesian coordinates:

```
    O         0.000000     0.000000     0.114419
    H         0.000000     0.762474    −0.457677
    H         0.000000    −0.762474    −0.457677
```

Absolute energy: −76.393378

Frequencies: 1637 3975 4101

TS2a

Cartesian coordinates:

```
    C         0.105663     0.009292    −0.046889
    H        −0.886516     0.094749     0.394090
    H         0.839250     0.190865     0.738038
```

```
      H          0.247734    -0.994864    -0.440503
      O          0.324451     0.990364    -1.010782
      H         -0.092083     0.705794    -1.960623
      O         -1.126152     0.525054    -2.634691
      H         -1.595439     1.364302    -2.608497
```

Absolute energy: -191.365423

Frequencies:

```
   -1737        119         181
     247        422         782
    1110       1161        1194
    1338       1480        1493
    1536       1611        3094
    3174       3192        3932
```

TS2b

Cartesian coordinates:

```
      C          0.002009    -0.002144    -0.016312
      H         -0.198008    -0.074084     1.046477
      H          1.069315     0.113107    -0.205404
      H         -0.268890    -1.025812    -0.482710
      O         -0.772305     1.011181    -0.541266
      H         -0.541478     1.154879    -1.456222
      O         -0.791077    -2.204250    -1.161656
      H         -1.718987    -2.054887    -0.943028
```

Absolute energy: -191.368685

Frequencies:

```
    -437         89         148
     244        445         753
    1085       1148        1193
    1373       1415        1477
    1513       1728        3125
    3239       3890        3995
```

S2. Equilibrium constants

The equilibrium constant, $K_{eq,D}$, for the process 2M ↔ D, where M and D are methanol monomer and dimer, respectively, were calculated using the MPWB1K/6-31+G(d,p) information. Specifically,

$$K_{eq,D} = \frac{2Q_{rot,D}Q_{vib,D}Q_{el,D}}{\left(Q_{rot,M}Q_{vib,M}Q_{el,M}\right)^2 \Phi_{rel}} e^{-\beta V_0} \tag{S1}$$

where $Q_{rot,X}Q_{vib,X}Q_{el,X}$ is the product of the rotational, vibrational and electronic partition functions of the monomer (X = M) and dimer (X = D), respectively. The difference in energy between the two monomers and the dimer is V_0 = 6.10 kcal/mol.

The zero-point energy contributions are included in the vibrational partition functions. The relative translation motion of the two reactants is given by

$$\Phi_{rel} = \left(\frac{2\pi\mu_{rel}}{\beta h^2}\right)^{3/2} \tag{S2}$$

where μ_{rel} is the reduced mass of the two fragments; h is Planck constant and $\beta=1/k_BT$, k_B being Boltzmann constant. The factor of 2 in eq S1 arises from the fact that the two reactants correspond to identical molecules.

The equilibrium constant is also given by:

$$K_{eq,D} = \frac{[D]}{[M]^2} \tag{S3}$$

and $[Met] = [M] + 2[D]$, where $[Met]$ is the total concentration of methanol. If x represents the fraction of molecules of monomer, i.e., $x = [M]/[Met]$ the following equation is obtained:

$$2K_{eq,D}[Met]x^2 + x - 1 = 0 \tag{S4}$$

Eq S4 allows the calculation of x using the equilibrium constant values of eq S1 and a given concentration of methanol. For a concentration of 5×10^{14} molecules/cm^3 the values the monomer's fraction is indicated below:

```
  T(K)    Monomer's fraction
 50.00       0.00
 56.00       0.00
 65.00       0.05
 75.00       0.67
 80.00       1.83
 82.00       2.65
 88.00       7.07
100.00      31.31
112.00      71.85
120.00      89.34
123.00      92.86
125.00      94.55
130.00      97.20
138.00      98.97
143.00      99.42
150.00      99.73
163.00      99.92
175.00      99.97
180.00      99.98
200.00     100.00
202.00     100.00
```

S3. Small-curvature tunneling probabilities

OH channel

P(E) starts at the ZPE (39.13 kcal/mol) of the methanol···OH complex

E(Kcal/mol)	P(E)
39.127	0.393760E-14
39.133	0.406670E-14
39.144	0.434290E-14
39.160	0.479900E-14
39.182	0.548290E-14
39.209	0.647780E-14
39.242	0.792310E-14
39.280	0.100420E-13
39.323	0.131970E-13
39.371	0.180010E-13
39.424	0.255310E-13
39.483	0.377370E-13
39.546	0.582880E-13
39.614	0.944670E-13
39.687	0.161800E-12
39.765	0.297320E-12
39.847	0.609980E-12
39.934	0.129930E-11
40.024	0.279840E-11
40.119	0.613210E-11
40.218	0.136090E-10
40.321	0.304510E-10
40.427	0.698850E-10
40.537	0.164310E-09
40.650	0.386720E-09
40.767	0.894930E-09
40.886	0.203990E-08
41.008	0.467690E-08
41.133	0.106370E-07
41.261	0.255550E-07
41.390	0.607620E-07
41.522	0.150980E-06
41.656	0.325280E-06
41.791	0.673380E-06
41.928	0.131790E-05
42.066	0.252050E-05
42.205	0.464220E-05
42.345	0.878950E-05
42.485	0.164470E-04
42.626	0.298110E-04
42.767	0.534510E-04
42.909	0.947450E-04
43.049	0.164570E-03
43.190	0.278240E-03
43.330	0.460390E-03
43.469	0.746490E-03
43.607	0.118770E-02

```
43.744   0.185400E-02
43.879   0.283650E-02
44.013   0.425010E-02
44.144   0.623460E-02
44.274   0.895790E-02
44.401   0.126350E-01
44.526   0.175460E-01
44.649   0.240020E-01
44.768   0.322850E-01
44.884   0.426520E-01
44.998   0.553500E-01
45.108   0.706170E-01
45.214   0.886280E-01
45.317   0.109500
45.416   0.133330
45.510   0.160180
45.601   0.189920
45.688   0.222140
45.770   0.255590
45.847   0.288180
45.920   0.318780
45.989   0.347320
46.052   0.373500
46.110   0.396920
46.164   0.417500
46.212   0.435430
46.255   0.450890
46.293   0.463960
46.326   0.474760
46.353   0.483420
46.375   0.490120
46.391   0.495010
46.402   0.498160
46.407   0.499700
46.410   0.500000
46.413   0.500300
46.418   0.501840
46.429   0.504990
46.445   0.509880
46.467   0.516580
46.495   0.525240
46.527   0.536040
46.565   0.549110
46.608   0.564570
46.656   0.582500
46.710   0.603080
46.768   0.626500
46.831   0.652680
46.900   0.681220
46.973   0.711820
47.050   0.744410
47.132   0.777860
47.219   0.810080
47.310   0.839820
47.404   0.866670
```

```
47.503   0.890500
47.606   0.911372
47.712   0.929383
47.822   0.944650
47.936   0.957348
48.052   0.967715
48.171   0.975998
48.294   0.982454
48.419   0.987365
48.546   0.991042
48.676   0.993765
48.807   0.995750
48.941   0.997163
49.076   0.998146
49.213   0.998812
49.351   0.999254
49.490   0.999540
49.630   0.999722
49.771   0.999835
49.912   0.999905
50.053   0.999947
50.194   0.999970
50.335   0.999984
50.475   0.999991
50.615   0.999995
50.754   0.999997
50.892   0.999999
51.029   0.999999
51.164   1.000000
51.298   1.000000
51.430   1.000000
51.559   1.000000
51.687   1.000000
51.812   1.000000
51.934   1.000000
52.053   1.000000
52.170   1.000000
52.283   1.000000
52.393   1.000000
52.499   1.000000
52.602   1.000000
52.701   1.000000
52.796   1.000000
52.886   1.000000
52.973   1.000000
53.055   1.000000
53.133   1.000000
53.206   1.000000
53.274   1.000000
53.337   1.000000
53.396   1.000000
53.449   1.000000
53.497   1.000000
53.540   1.000000
53.578   1.000000
```

```
53.611  1.000000
53.638  1.000000
53.660  1.000000
53.676  1.000000
53.687  1.000000
```

CH3 channel
```
39.048  0.102040E-19
39.053  0.104420E-19
39.062  0.109430E-19
39.077  0.117480E-19
39.096  0.129120E-19
39.120  0.145240E-19
39.149  0.167270E-19
39.183  0.197250E-19
39.221  0.238130E-19
39.264  0.294250E-19
39.311  0.372220E-19
39.363  0.482030E-19
39.419  0.638970E-19
39.480  0.866950E-19
39.545  0.120400E-18
39.614  0.171170E-18
39.686  0.249090E-18
39.763  0.371010E-18
39.844  0.565670E-18
39.928  0.882880E-18
40.016  0.141060E-17
40.107  0.230720E-17
40.201  0.386360E-17
40.299  0.662500E-17
40.399  0.116340E-16
40.503  0.209300E-16
40.609  0.385830E-16
40.717  0.729170E-16
40.828  0.141340E-15
40.941  0.281150E-15
41.056  0.574440E-15
41.173  0.120690E-14
41.292  0.261150E-14
41.412  0.583180E-14
41.533  0.134780E-13
41.655  0.323870E-13
41.779  0.817230E-13
41.903  0.224060E-12
42.028  0.613360E-12
42.153  0.171600E-11
42.278  0.501600E-11
42.403  0.158710E-10
42.528  0.522520E-10
42.653  0.168710E-09
42.777  0.537150E-09
42.901  0.174580E-08
43.023  0.585610E-08
43.144  0.175500E-07
```

```
43.264    0.509870E-07
43.383    0.152520E-06
43.500    0.427360E-06
43.615    0.108230E-05
43.728    0.274820E-05
43.839    0.716750E-05
43.947    0.189470E-04
44.053    0.432200E-04
44.157    0.955620E-04
44.257    0.208700E-03
44.355    0.445620E-03
44.449    0.907570E-03
44.540    0.175420E-02
44.628    0.325470E-02
44.712    0.582300E-02
44.793    0.100500E-01
44.870    0.167290E-01
44.942    0.268510E-01
45.011    0.415400E-01
45.076    0.618460E-01
45.137    0.885610E-01
45.193    0.121880
45.245    0.161250
45.292    0.205360
45.335    0.252320
45.373    0.299910
45.407    0.345750
45.436    0.387590
45.460    0.423800
45.479    0.453490
45.494    0.476110
45.503    0.491120
45.508    0.498530
45.530    0.500000
45.552    0.501470
45.557    0.508880
45.566    0.523890
45.581    0.546510
45.600    0.576200
45.624    0.612410
45.653    0.654250
45.687    0.700090
45.725    0.747680
45.768    0.794640
45.815    0.838750
45.867    0.878120
45.924    0.911439
45.984    0.938154
46.049    0.958460
46.118    0.973149
46.191    0.983271
46.267    0.989950
46.348    0.994177
46.432    0.996745
46.520    0.998246
```

```
46.611  0.999092
46.705  0.999554
46.803  0.999791
46.903  0.999904
47.007  0.999957
47.113  0.999981
47.221  0.999993
47.332  0.999997
47.445  0.999999
47.560  1.000000
47.677  1.000000
47.796  1.000000
47.916  1.000000
48.037  1.000000
48.159  1.000000
48.283  1.000000
48.407  1.000000
48.532  1.000000
48.657  1.000000
48.782  1.000000
48.907  1.000000
49.032  1.000000
49.157  1.000000
49.281  1.000000
49.405  1.000000
49.527  1.000000
49.649  1.000000
49.769  1.000000
49.887  1.000000
50.004  1.000000
50.119  1.000000
50.232  1.000000
50.343  1.000000
50.452  1.00000
50.558  1.00000
50.661  1.00000
50.761  1.00000
50.859  1.00000
50.953  1.00000
51.044  1.00000
51.132  1.00000
51.216  1.00000
51.297  1.00000
51.374  1.00000
51.447  1.00000
51.515  1.00000
51.580  1.00000
51.641  1.00000
51.697  1.00000
51.749  1.00000
51.796  1.00000
51.839  1.00000
51.877  1.00000
51.911  1.00000
51.940  1.00000
```

```
51.964    1.00000
51.983    1.00000
51.998    1.00000
52.008    1.00000
52.012    1.00000
```

S4. Details on the dynamics calculations

The kinetics of the methanol + OH reaction has been studied by a combination of quasi-classical trajectories (QCT), Rice-Rampsperger-Kassel-Markus (RRKM) calculations including small-curvature tunneling (SCT) corrections (RRKM/SCT), and Kinetic Monte Carlo (KMC) simulations.[3] In addition to studying the methanol monomer (M) + OH reaction, the possible presence of methanol clusters in the reaction chamber, and in particular dimers (D), is analyzed.

The reaction mechanism can be studied by splitting it into different processes. The first one is an association or capture process (R1) leading to an activated OH···O(H)CH$_3$ complex C. And then, dissociation (R-1) or hydrogen abstraction reactions (R2) from C will compete:

$$M(D) + OH \xrightarrow{k_{1,M/D}} C(+M) \tag{R1}$$

$$C \xrightarrow{k_{-1}} M + OH \tag{R-1}$$

$$C \xrightarrow{k_{2a}} H_2O + CH_2OH \tag{R2a}$$

$$C \xrightarrow{k_{2b}} H_2O + CH_3O \tag{R2b}$$
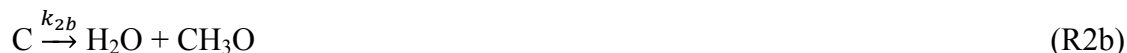
As detailed below, QCT simulations were employed to determine $k_{1,M/D}$ and to study the internal energy content of the nascent complex, while RRKM calculations were employed to obtain k_{-1}, k_{2a} and k_{2b}. For the reactions that involve H transfer (R2a and R2b), tunneling probabilities calculated with the small curvature (SCT) approach are employed.

A total rate coefficient for the hydrogen abstraction reactions k_2 can be defined as $k_2 = k_{2a} + k_{2b}$. Finally, KMC simulations are carried out to determine the total bimolecular rate for product formation, and to analyze pressure effects.

S4.1. Analytical potential energy function

The RRKM calculations employ the above tunneling results and electronic structure results. For the QCT simulations an analytical potential energy function was built, fitted to MPWB1K/6-31+G(d,p) calculations.

M + OH system. The analytical function for the M + OH system reads:

$$V_{M+OH} = V_{intra,M+OH} + V_{inter,M+OH} \tag{S1}$$

Where $V_{intra,\text{M+OH}}$ comprises the CH_3OH and OH potential energy functions, and $V_{inter,\text{M+OH}}$ is the interaction potential between methanol and OH. $V_{intra,\text{M+OH}}$ is expressed as:

$$V_{intra,\text{M+OH}} = \sum_{i=1}^{6} 1/2 k_i^s (r_i - r_i^0)^2 + \sum_{j=1}^{7} 1/2 k_i^b (\theta_i - \theta_i^0)^2 + V_0 \sum_{k=1}^{3} \cos^2(3\tau_k/2)$$

(S5)

Where k^s and k^b are the stretching and bending force constants, r_i^0 and θ_i^0 are the equilibrium bond lengths and angles, respectively, and the last three terms represent the potential function for the 3-fold torsion, as a function of the three dihedral angles $\tau_k = H_iCOH$ ($i = 1$, 3 and 4). The labels of the atoms are shown in Figure S1.

The parameters of the intramolecular part of the potential are gathered in Table S1, as well as a comparison of the MPWB1K/6-31+G(d,p) vibrational frequencies of M and OH with those obtained with the analytical function.

Table S1: Parameters of the intramolecular part of the potential energy function

Stretching force constants (k_i^s)	Value (mdyn/Å)
CH_i	5.300
CC	6.000
OH (methanol)	8.420
OH (hidroxy)	8.126
Equilibrium bond lengths (r_i^0)	Value (Å)
CH_i	1.090
CC	1.408
OH (methanol)	0.954
OH (hidroxy)	0.976
Bending force constants (k_i^b)	Value (mdynÅ/rad^2)
H_iCO	1.10
H_iCH_j	0.40
COH	1.00
Equilibrium bond angles (θ_i^0)	Value (degrees)
H_iCO	109.47
H_iCH_j	109.47
COH	110.55
Torsion parameter V_0	Value (kcal/mol)
H_iCOH	0.390
Vibrational frequencies of methanol (in cm^{-1})	
MPWB1K/6-31+G(d,p)	Analytical function
324; 1085; 1146; 1206; 1385; 1518; 1534; 1545; 3086; 3148; 3220; 4011	324; 1059; 1156; 1170; 1412; 1438; 1517; 1697; 3049; 3168; 3170; 3898
Vibrational frequency of OH (in cm^{-1})	
MPWB1K/6-31+G(d,p)	Analytical function
3865	3828

The intermolecular part of the analytical PES is built using Morse potentials and two-body repulsion and dispersion terms, both corrected with angular functions.

$$V_{inter,\text{M+OH}} = \sum_{i=1}^{2}\{D_{e,i}\{1 - \exp\left[-\beta_i(r_i - r_i^0)\right]\}^2 - D_{e,i}\}f_i(\theta_k, \theta_l, \theta_m, \theta_n, \theta_p, \theta_q, \theta_r) +$$

$$\sum_{j=1}^{8}\left\{A_j \exp(-B_j r_j) + \frac{C_j}{r_j^{D_j}} + \frac{E_j}{r_j^{F_j}}\right\}g_j(\theta_k, \theta_l, \theta_m, \theta_n, \theta_p, \theta_q, \theta_r) \tag{S6}$$

Where the two Morse potentials refer to the O_5–H_7 and O_8–H_6 distances, respectively (see Figure S1 for the labels), and the eight Buckingham-type two-body terms refer to the H_1–H_7, H_3–H_7, H_4–H_7, H_1–O_8, H_3–O_8, H_4–O_8, O_5–O_8, H_6–H_7 distances, respectively. To add flexibility to the Morse potential, β_i parameters depend on the r_i distance:

$$\beta_i = b_{0,i} + b_{1,i}(r_i - r_i^0) + b_{2,i}(r_i - r_i^0)^2 \tag{S7}$$

The hydrogen bonds that stabilize the complex formed in this system are highly directional, and each of the above intermolecular terms is multiplied by the functions $f_i(\theta_k, \theta_l, \theta_m, \theta_n, \theta_p, \theta_q, \theta_r)$ and $g_i(\theta_k, \theta_l, \theta_m, \theta_n, \theta_p, \theta_q, \theta_r)$ that depend on seven different angles:

$$f_1 = f_2 = h_1 = \prod_{i=1}^{3} \exp\left[-a_i(\theta_i^0 - \theta_i)^2\right] \tag{S8}$$

$$h_2 = \exp[-a_4(\theta_4^0 - \theta_4)^2]\times\exp[-a_{51}(\theta_5^0 - \theta_5) - a_{54}(\theta_5^0 - \theta_5)^4 - a_{56}(\theta_5^0 - \theta_5)^6]$$
$$\tag{S6}$$

$$g_1 = g_2 = g_3 = 1 - \prod_{i=6}^{7} \exp\left[-a_i(\theta_i^0 - \theta_i)^2\right] \tag{S9}$$

$$g_4 = g_5 = g_6 = \prod_{i=6}^{7} \exp\left[-a_i(\theta_i^0 - \theta_i)^2\right] \tag{S10}$$

$$g_7 = g_8 = (1 - h_1)(1 - h_2) \tag{S11}$$

The seven different angles θ_i are $O_5\cdots H_7$–O_8, O_5–$H_6\cdots H_7$, C_2–$O_5\cdots H_7$, $H_6\cdots O_8$–H_7, O_5–$H_6\cdots O_8$, C_2–$O_5\cdots O_8$, $C_2\cdots O_8$–H_7, for $i = 1, 7$, respectively. In turn, parameters a_4 and a_{5j} ($j = 1, 4$ and 6) also depend on θ_4 and on the O_8–H_6–O_5–C_2 torsion (τ), respectively:

$$a_4 = a_{40} + a_{41}\times(\pi - \theta_4) \tag{S12}$$

$$a_{5j} = a_{5j}^0 + a_{5j}^1\times[0.5\times(1 + \cos(\tau))] \tag{S13}$$

This analytical function was fitted to around 1400 MPWB1K/6-31+G(d,p) single point energy data for several orientations of the hydroxyl radical with respect to methanol (see Figure S1). The fits were conducted with the help of a genetic algorithm.
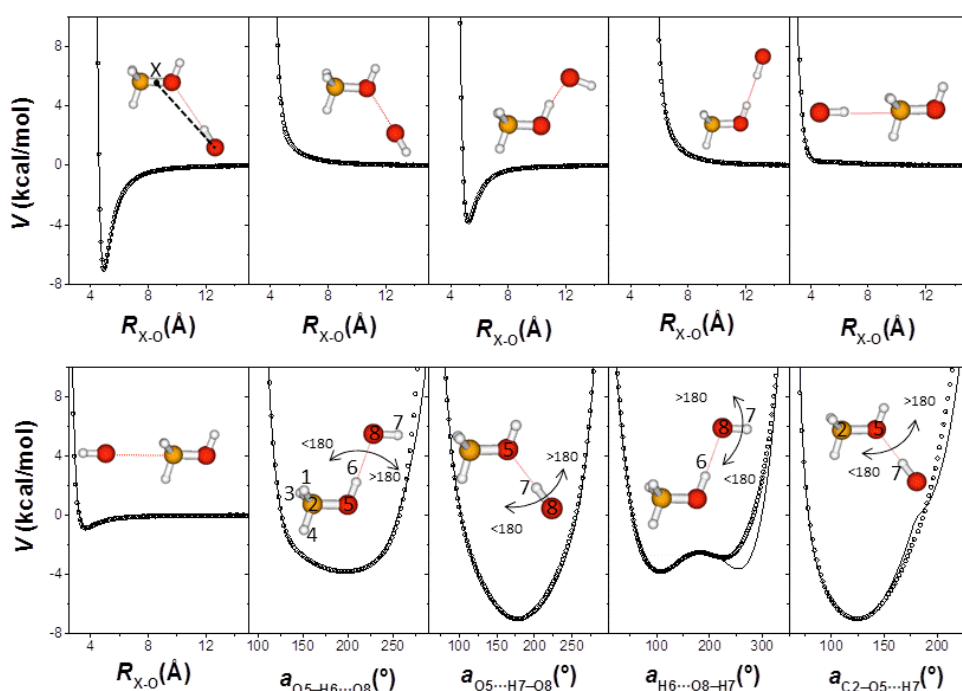
Figure S1. Fits of the analytical PES employed to study M + OH collisions (solid line) to MPWB1K/6-31+G(d,p) single point calculations (circles). For the distances shown in the *x*-axes, X represents the middle point of the C–O bond, and O represents the oxygen atom of the hydroxyl radical as indicated in the upper left plot.

The optimized intermolecular parameters of the potential function are collected in Table S2, alongside with the vibrational frequencies of C. Figure S2 shows the geometry of the complex obtained with the potential function developed here, in comparison with the MPWB1K/6-31+G(d,p) geometry.

Table S2: Parameters of the intermolecular part of the potential energy function

$D_{e,i}$ (kcal/mol)	
O_5–H_7	6.973
O_8–H_6	3.300
r_i^0 (Å)	
O_5–H_7	1.868
O_8–H_6	2.082
$b_{0,i}$ (Å^{-1})	
O_5–H_7	1.462
O_8–H_6	1.500
$b_{1,i}$ (Å^{-2})	
O_5–H_7	-0.185
O_8–H_6	-0.119
$b_{2,i}$ (Å^{-3})	
O_5–H_7	0.010
O_8–H_6	0.003

a_i	
a_1	0.30 rad^{-2}
a_2	0.30 rad^{-2}
a_3	0.30 rad^{-2}
a_{40}	0.09 rad^{-2}
a_{41}	0.30 rad^{-3}
a_{51}^0	0.00 rad^{-1}
a_{51}^1	0.30 rad^{-1}
a_{54}^0	0.14 rad^{-4}
a_{54}^1	-0.14 rad^{-4}
a_{56}^0	0.04 rad^{-6}
a_{56}^1	0.40 rad^{-6}
a_6	0.15 rad^{-2}
a_7	0.20 rad^{-2}
A_j (kcal/mol)	
H_i–H_7	1773.98
H_i–O_8	0.00
O_5–O_8	30624.83
H_6–H_7	538357.42
B_j (Å^{-1})	
H_i–H_7	3.912
H_i–O_8	0.000
O_5–O_8	4.110
H_6–H_7	47.300
C_j (kcal/molÅ^{D_j})	
H_i–H_7	0.000
H_i–O_8	-60.000
O_5–O_8	1200000.000
H_6–H_7	40.010
D_j	
H_i–H_7	-
H_i–O_8	3.700
O_5–O_8	20.500
H_6–H_7	3.215
E_j (kcal/mol^{F_j})	
H_i–H_7	200.000
H_i–O_8	3150.799
O_5–O_8	61.454
H_6–H_7	0.000
F_j	
H_i–H_7	12.038
H_i–O_8	8.146
O_5–O_8	2.798
H_6–H_7	-
Vibrational frequencies of C (in cm^{-1})	
MPWB1K/6-31+G(d,p)	Analytical function
33; 60; 196; 308; 438; 631; 1063; 1092; 1163; 1340; 1464; 1479; 1490; 2996; 3068; 3120; 3563; 3867	40; 96; 209; 238; 342; 527; 1061; 1158; 1170; 1418; 1438; 1538; 1699; 3049; 3168; 3170; 3898; 3907

MPWB1K/6-31+G(d,p)   Analytical function

$O_8H_6O_5C_2$ = 159.2 degrees

1.846
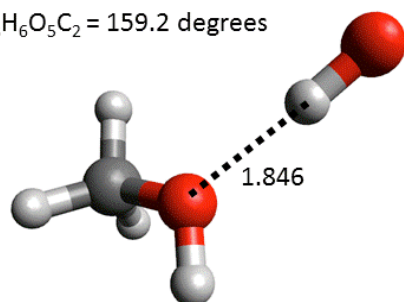
E_{int} = 7.49 kcal/mol

$O_8H_6O_5C_2$ = 157.6 degrees

1.868
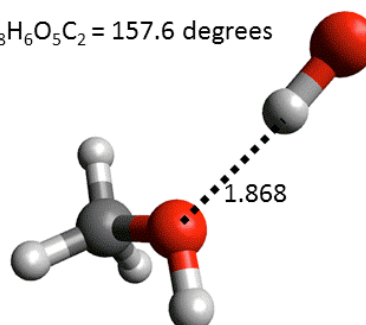
E_{int} = 7.02 kcal/mol

Figure S2. Minimum energy structures of the complex.

D + OH system. The potential energy function employed in the D + OH simulations is the same as above, but including some extra terms:

$$V_{D+OH} = V_{intra,D+OH} + V_{inter,D+OH} \tag{S14}$$

Where $V_{intra,D+OH}$ includes the above intramolecular terms of eq S5 for the second methanol molecule, and $V_{inter,D+OH}$ reads:

$$V_{inter,D+OH} = V_{inter,M_1+OH} + V_{inter,M_2+OH} + V_D \tag{S15}$$

Where $V_{inter,OH+M_1}$ and $V_{inter,OH+M_2}$ refer to the interaction of OH with each methanol monomer (labelled as 1 and 2) and they are the same as above (eq S6).

An additional term V_D is needed to account for the intermolecular interactions within the dimer. This potential function was taken from the literature[4] and it accurately describes the global minimum of the dimer as depicted in Figure S3. The minimum energy structure obtained with V_D was optimized using the standard options of the chemical dynamics program VENUS.[5]

MPWB1K/6-31+G(d,p)   **Analytical function**

1.899   1.966

E_{int} = 6.10 kcal/mol E_{int} = 5.12 kcal/mol
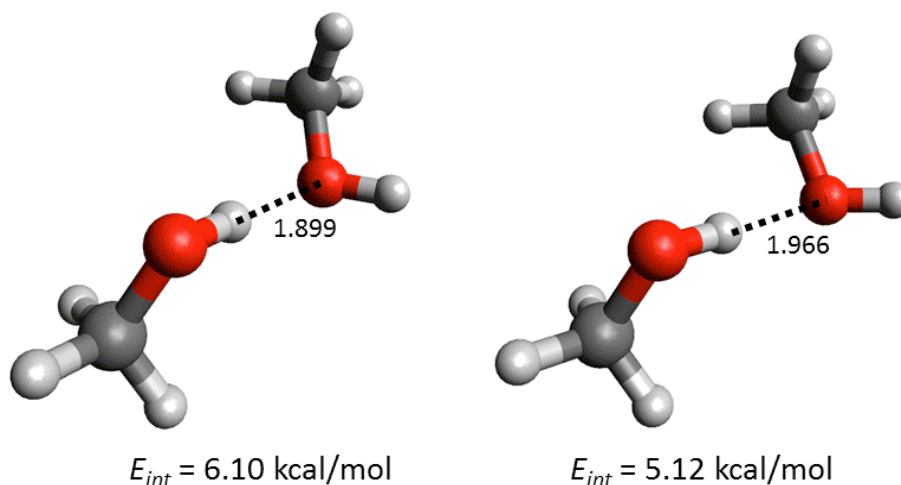
Figure S3. Minimum energy structures of methanol dimer.

S4.2. Capture rate coefficients

Capture rate coefficients $k_{1,M/D}(T)$ were calculated at the following temperatures: 50, 100, 150 and 200 K for M(D) + OH using QCT simulations. Ro-vibrational energies are assigned to the reactants according to a Maxwell-Boltzmann distribution of states, and the maximum impact parameter was set to 13.2 Å. Batches of 5×10^4 trajectories were run for each temperature to calculate the capture rates according to the following expression:

$$k_{1,M/D}(T) = \frac{2}{2+2\exp{(-205/T)}} \left(\frac{8kT}{\pi\mu}\right)^{1/2} \pi b_{max}^2 \left(\frac{N_c}{N_t}\right) \tag{S16}$$

where the first factor represents the ratio of the electronic partition functions, μ is the reduced mass for the M(D) + OH system, N_t is the total number of trajectories, and N_c is the number of capture trajectories. The criterion to decide whether a trajectory leads to capture was geometric, i.e., those trajectories for which, at same point, the $O_5\cdots H_7$ distance drops below 2 Å were regarded as capture. For a number of capture trajectories the second most stable $CH_3OH\cdots OH$ complex was also formed. The QCT simulations have been carried out with the chemical dynamics program VENUS.[5] Table S3 collects the rate coefficients obtained using the above procedure.

Table S3: Capture rate coefficients $k_{1,M/D}$ obtained in this study.

T (K)	$k_{1,M}$ (10^{-10} cm^3 molecule^{-1}s^{-1})	$k_{1,D}$ (10^{-10} cm^3 molecule^{-1}s^{-1})
50	2.78	4.99
100	2.33	4.89
150	2.13	4.46
200	1.74	4.12

S4.3 Survival probabilities and internal energy content of the nascent complexes

Survival probabilities of C. The complexes formed in the capture step are highly vibrationally excited and can redissociate back to the reactants. The survival probabilities $P(t) = N(t)/N(0)$ of nascent C, where $N(t)$ is the number of complexes that survive at time t, are depicted in Figure S4 for the different temperatures. The survival time t is computed here as the difference between the first and last time the $O_5\cdots H_7$ distance drops below 2 Å. Batches of 5×10^4 trajectories were run to compute the $P(t)$ plots.
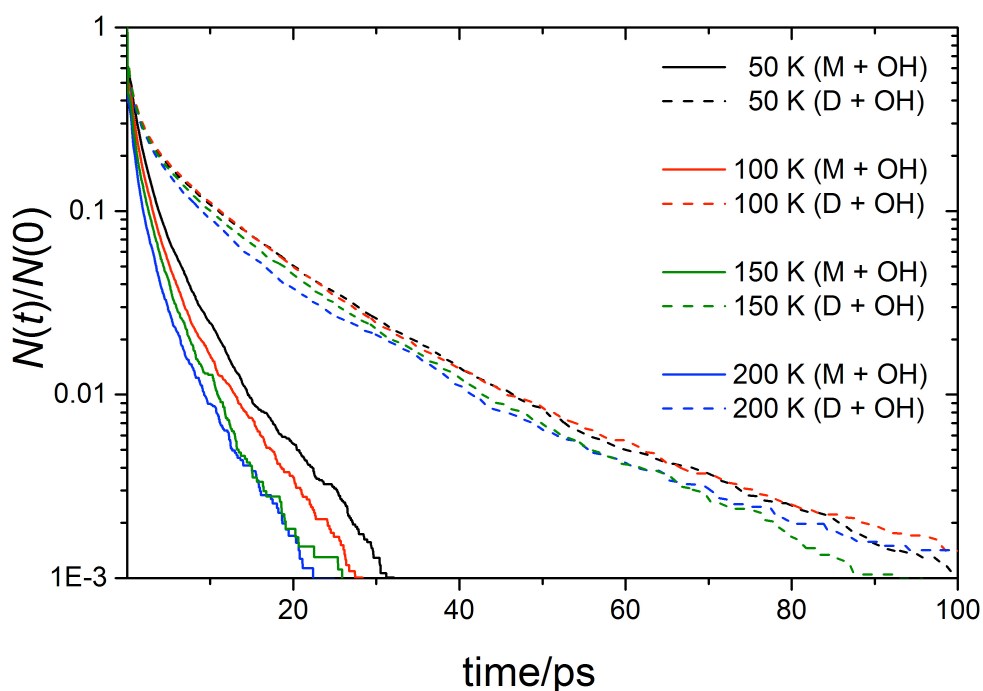
Figure S4. Survival probabilities of C obtained in the QCT simulations for M + OH (solid lines) and D + OH (dashed lines)

According to our QCT simulations, the survival probabilities are highly non-RRKM, i.e., nonexponential, and similar to those obtained in related processes.[6] The non-linear

behavior of the above $P(t)$ plots might be a consequence of slow intramolecular vibrational redistribution (IVR). However, the substantial zero-point energy (ZPE) leakage that affects our QCT simulations prevents us from drawing a definite conclusion.

At any rate, Figure S4 points out to a much longer survival probabilities of the nascent complexes formed in D + OH collisions. As explained in detail below, this can be understood in terms of a *substitution* mechanism, where the leaving methanol molecule carries away some energy, effectively cooling down the complexes.

The values of the dissociation rate constants k_{-1} could be computed from the above $P(t)$ plots as:

$$k_{-1}(t) = -\frac{d ln[P(t)]}{dt} \tag{S17}$$

However, since ZPE leakage severely affects the QCT simulations, we opted here to employ variational RRKM theory to determine the dissociation rates. To asses ZPE leakage more quantitatively, the vibrational energies of OH and CH$_3$OH, obtained after dissociation of C, have been computed for the lowest temperature of 50 K.

Figure S5 shows the percent vibrational energy variation in M + OH capture trajectories at 50 K. As seen in the figure, almost 90% of the trajectories end without their ZPE. However, when the simulations are carried out without the ZPE (only initial relative translational and rotational energies are given to M and OH) for a maximum time of 1 ns and T = 50 K, all the capture trajectories survive until the end of the simulation. This result indicates that QCT is not suitable to compute dissociation rates at energies close to the threshold.
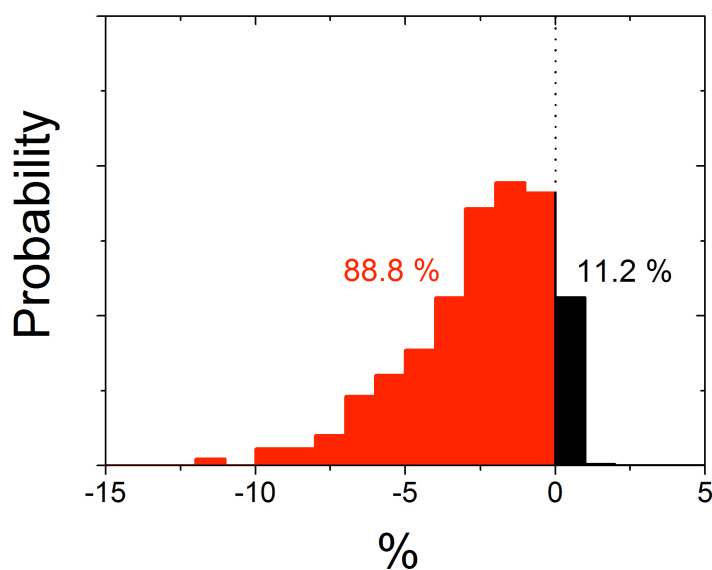
Figure S5. Percent vibrational energy variation in the M + OH at 50 K.

Internal energy content of C. The internal energy distribution of the complexes formed in M + OH collisions and in D + OH collisions differ substantially between each other. This difference explains the much higher bimolecular rates found in this study for the D + OH reaction as indicated below.

In particular, M + OH collisions lead to complexes having the internal energy distributions $P_M^T(E)$ shown in red in Figure S6. By contrast, when OH collides with a dimer, the resulting distribution is much cooler (blue line in Figure S6), thanks to a *substitution* mechanism, where hydroxyl replaces one monomer, which carries off an amount of energy.

As detailed below, this is the major D + OH mechanism. For the *substitution* trajectories, the probability distribution functions $P_D^T(E)^0$ of the internal energy states of the nascent complex have been calculated (blue line in Figure S6). These distributions are well fit by Gaussian functions with average values of -2.06, -1.68, -0.78 and 0.09 kcal/mol (with respect to the M + OH dissociation limit) for 50, 100, 150 and 200 K, respectively. The dissociation energy of the complex is $\Delta E_0^0 = 5.64$ kcal/mol and Figure S6 shows relative energies with respect to the ZPE of the complex. The full widths at half maximum (FWHM) of the distributions are 14.0, 14.6, 14.9 and 15.9 kcal/mol, for 50, 100, 150 and 200 K, respectively.

As mentioned above, the M + OH simulations suffer from severe ZPE leakage, and the D + OH simulations are not an exception. In fact, the $P_D^T(E)^0$ distributions of Figure S6 show that an important fraction of complexes have internal energies below the ZPE. Nevertheless, quite clearly, the D + OH process leads to much cooler complexes, compared to the M + OH trajectories, which results in a higher bimolecular rate (*vide infra*).
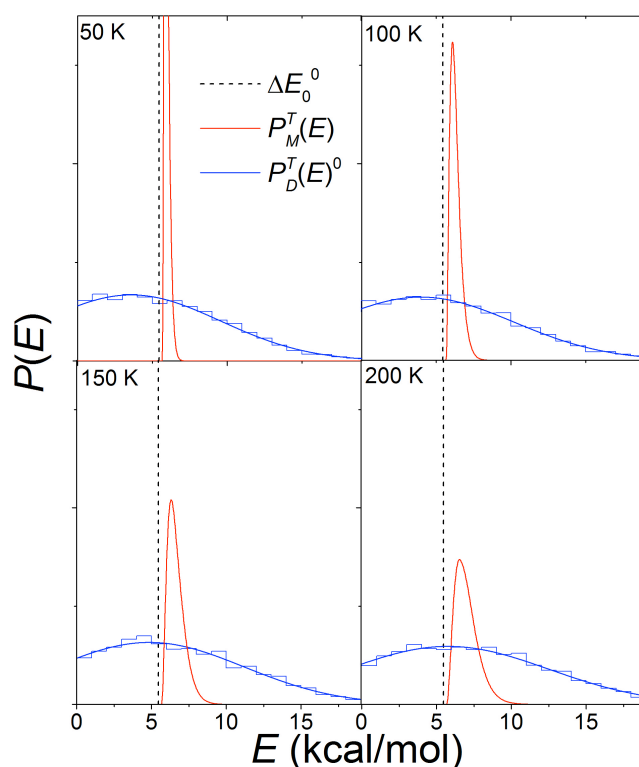
Figure S6. Internal energy distributions of the nascent complexes in D + OH collisions (blue) and M + OH collisions (red). The vertical dashed line indicates the dissociation energy of the complex ($\Delta E_0^0 = 5.64$ kcal/mol). The distributions are not normalized.

A detailed analysis of our D + OH simulations indicates that the trajectories can be classified according to two different mechanisms:

1) *Inelastic scattering*: D + OH → D′ + OH′
   In these trajectories, the dimer survives the collision with OH, and, therefore, they do not lead to an enhancement of the overall rate constant. The only effect of the interaction is an energy exchange between D and OH. The prime indicates a change in the internal energy content.

2) *Substitution*: D + OH → C + M
   The leaving methanol molecule carries away a fraction of the initial energy (see Figure S6). This mechanism can, in turn, be subdivided in two, according to whether:

   2.1. Hydroxyl only interacts with one methanol molecule.

   2.2. Hydroxyl interacts with both methanol molecules, eventually picking one to form the complex.

The *substitution* mechanism clearly dominates and accounts for 72%, 69%, 68% and 68% of the total, at 50, 100, 150 and 200 K, respectively. Additionally, 37%, 34%, 31% and 28% of the OH radicals interact with both methanol molecules at 50, 100, 150 and

200 K, respectively. Three representative movies of each type are enclosed in this Supporting Information.

Substitution enhances the overall bimolecular rate as a consequence of the cooling effect of the complex. This will hinder (or suppress) redissociation back to reactants, and will enhance the H abstraction processes (via tunneling).

S4.4 Overall rate coefficients

To compute the rates for the overall process:

$$M \,(D) + OH \xrightarrow{k_{M/D}} \text{products}$$
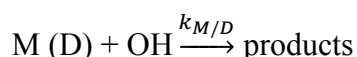
a series of KMC simulations were carried out, where the phase space is discretized, using a grain size of 10 cm^{-1}. In the following, a description of how each state to state rate was computed is described.

Collisional energy transfer rates are calculated using an exponential down model, with a value of 250 cm^{-1} for $< \Delta E_{down} >$ with N$_2$ gas densities in the range 0-17×10^{16} cm^{-3} molecule. The Lennard-Jones parameters needed to compute the collision frequency, as well as the above value for $< \Delta E_{down} >$, are taken from Shannon et al.[7]

For M + OH association reaction, the capture rate was fit to the following expression

$$k_{1,M}(T) = A_0 \left(\frac{T}{T_0}\right)^n \tag{S18}$$

with $n = -0.31$, $T_0 = 50$ K and $A_0 = 2.78 \times 10^{-10}$ cm^{3}molecule^{-1}s^{-1}. Using an inverse Laplace transform method, the microcanonical association rates, employed in the KMC simulation, can be obtained as[8]

$$k_{1,M}^T(E) =$$
$$\frac{A_0}{T_0^n \Gamma(n+1.5)} \left(\frac{2\pi\mu}{h^2}\right)^{3/2} \left\{ \int_0^E d\tau \rho_R(E-\tau)\,(\tau - \Delta H_0^0)^{n+0.5} u(\tau - \Delta H_0^0) \right\} \frac{\exp\left(-(E-\Delta E_0^0)/RT\right)}{Q_R(T)}$$
$$\tag{S17}$$

Which allow us to factorize the microcanonical rates as:

$$k_{1,M}^T(E) = k_{1,M}(T) P_M^T(E) \tag{S19}$$

Where the internal energy distribution function $P_M^T(E)$ reads

$$P_M^T(E) =$$
$$\left(\frac{2\pi\mu}{h^2}\right)^{3/2} \frac{1}{T^n \Gamma(n+1.5)} \left\{ \int_0^E d\tau \rho_R(E-\tau)\,(\tau - \Delta H_0^0)^{n+0.5} u(\tau - \Delta H_0^0) \right\} \frac{\exp\left(-(E-\Delta E_0^0)/RT\right)}{Q_R(T)}$$
$$\tag{S19}$$

Where Γ is the gamma function, ρ_R is the convolved rovibrational density of states of the reactants (M and OH), u is the Heavyside step function, $\Delta E_0^0 = 5.64$ kcal/mol, and $Q_R(T)$ is the total partition function (including translation) of the reactants.

For the D + OH simulations, the thermal capture rates are corrected with the fraction of the *substitution* trajectories at each temperature, assuming that the *inelastic scattering* process leads to fleeting complexes (trimers) that immediately redissociate, and therefore do not lead to products. The above Gaussian distributions $P_D^T(E)^0$ and the corresponding thermal rate constant for the dimer are employed to obtain the microcanonical association rates:

$$k_{1,D}^T(E) = k_{1,D}(T)P_D^T(E)^0 \qquad (S20)$$

Additionally, since the original Gaussians have tails that enter the quantum-mechanically forbidden region (below the ZPE of C), a set of KMC simulations was carried out using the modified Gaussian distributions $P_D^T(E)^1$ of Figure S7. The modified distributions have FWHM values 10 times smaller than the original ones, although their average values remain the same.
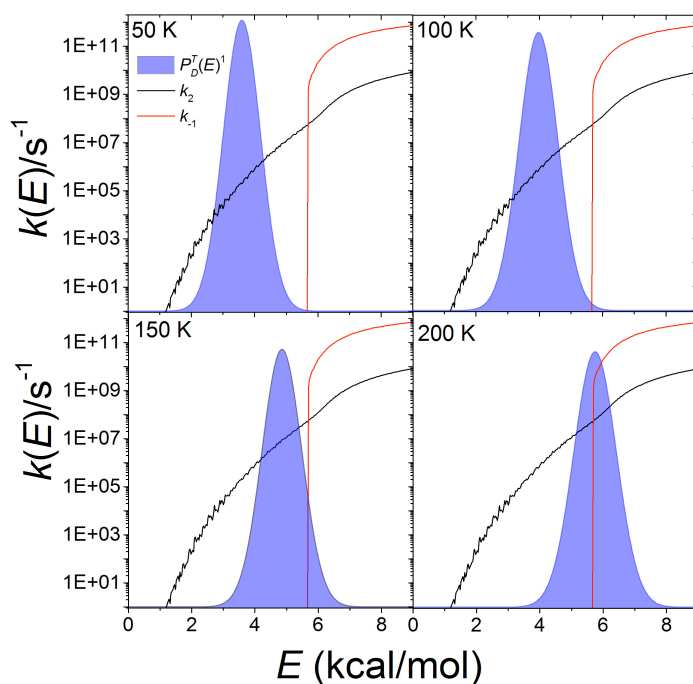
Figure S7. Modified Gaussian distribution $P_D^T(E)^1$ of the internal energy of the nascent C complexes in D + OH collisions (black line), together with the microcanonical rates (in s^{-1}) k_{-1} (red) and k_2 (blue).

The FWHM of $P_D^T(E)^1$ is somewhat arbitrary. However, as discussed below, the total bimolecular D + OH rates obtained with $P_D^T(E)^0$ and $P_D^T(E)^1$ fall within a relatively

narrow range of values, besides the large differences in the thickness of the distributions.

Figure S7 also shows the values of k_2 and k_{-1}, which are computed with RRKM theory; the latter using the variational prescription. In the calculation of k_{-1}, all the modes are treated as harmonic oscillators except the ones corresponding to the two lowest vibrational frequencies in the reactant and transition state, which are substituted by sterically-hindered two-dimensional rotors.[9] In particular, since the reactant rotors are more sterically-hindered than those of the variational transition state, the effective rotational constant of the reactant was chosen to be 1.6 greater than that of the transition state[9] to obtain the same rate constant as in ref 7 at 200 K.

Table S4 and Figure 4 of the manuscript show the total bimolecular rates obtained in this study for both the M + OH and D + OH reactions, using a bath gas (N$_2$) density of 5×10^{16} molecule cm^{-3}.

Table S4: Overall rate coefficients $k_{M/D}$ obtained in this work as a function of temperature.

T (K)	k_M (cm^{3}molecule^{-1}s^{-1})	k_D (cm^{3}molecule^{-1}s^{-1})	
		$P_D^T(E)^0$	$P_D^T(E)^1$
50	1.67×10^{-12}	1.82×10^{-10}	3.59×10^{-10}
100	0.99×10^{-12}	1.60×10^{-10}	3.36×10^{-10}
150	0.90×10^{-12}	1.41×10^{-10}	2.68×10^{-10}
200	0.80×10^{-12}	1.05×10^{-10}	1.23×10^{-10}

As seen in Figure S8, pressure effects are negligible, in good agreement with experiment. The figure shows the variation of the bimolecular rates with bath gas density (from 0 to 17×10^{16} molecule cm^{-3}) for a temperature of 82 K. The theoretical result at this temperature was obtained via an interpolation of the 50 K and 100 K results. Although the rates obtained for the M + OH reaction show a slight increase with pressure, since the D + OH rates are very close to the capture limit, the overall effect of pressure is negligible. An almost perfect match with experiment is obtained when we employ the same constant value for α of 0.30 (as in the main text), which provides a value of the dimer fraction in the Laval nozzle of $y = 0.146$ at 82 K.
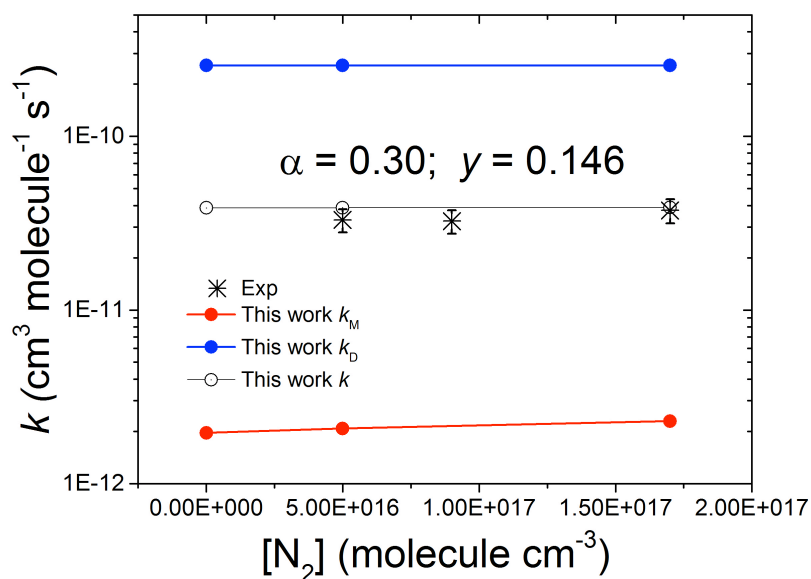
Figure S8. Variation of the Bimolecular rate coefficients with bath gas density at $T = 82$ K. The blue and red lines show the M + OH and D + OH results, respectively, while the black one is the averaged result, using a 14.6% fraction of D.

Finally, Table S5 lists the product branching ratios as a function of temperature, which agree satisfactorily with previous theoretical and experimental results.

Table S5: Abundances of methoxy radical product.

T (K)	Monomer	Dimer	Total
50	83.2	99.2	86.0
100	62.5	99.1	66.7
150	46.0	98.7	46.2
200	38.1	97.6	38.1

S5. Dependence of the pseudo-first order rates at high methanol concentrations

Overall, the pseudo-first order rates k' depend linearly on methanol concentration [Met]. However, a downward curvature is observed at very high values of [Met] by Gomez-Martin et al. (Ref. 8 of the manuscript), and also by other experimentalists[10] in related reactions, suggesting there is no equilibrium between methanol monomer and dimer.

That is because if there was an equilibrium, k' should display a linear or quadratic behavior with respect to [Met] as explained below.

If there is equilibrium between monomers and dimers: $2M \leftrightarrows D$, the following equilibrium constant K_p can be defined:

$$K_p = \frac{p_D}{p_M^2} \tag{S21}$$

and the dimer concentration would be obtained from $[D] = \frac{p_D}{RT} = K_p[M]^2RT$ (in units of mol/l).

Since the pseudo-first order rate can be written as a sum of the contributions from the monomer and dimer, with k_M and k_D being the corresponding bimolecular rates, one would obtain for k' the following final result:

$$k' = k_M[M] + k_D[D] = k_M[M] + k_D K_p[M]^2RT \tag{S22}$$

Therefore, assuming monomer-dimer equilibrium, and if the dimer were more reactive than the monomer, a quadratic dependence of k' on [M] would be obtained, like in the reaction of the Criegee radical with water.[11] By contrast, if the dimer were not very reactive (low k_D), one would observe a linear dependence of k' on [M].

However, Gomez-Martin et al. (Ref. 8 of the manuscript) observe a downward curvature of k' vs methanol concentration, and therefore the above equilibrium argument cannot be employed in the Laval nozzle experiments. In fact, dimers and other oligomers formed in supersonic expansions are not in equilibrium with the monomer, as detailed below.

Supersonic expansions using Laval nozzles are among the most widely used experimental techniques to study neutral gas phase nucleation.[12] The formation and growth of clusters is a complex process, which can be split in two different mechanisms:[13]

I.   *Formation of oligomers by monomer aggregation*

In the first stages after the gas mixture passes through the nozzle throat, when a sufficiently low temperature is attained, condensable gas monomers can bind together to form a dimer (this corresponds to a temperature smaller than the binding energy of the dimer). These dimers constitute seeds for further clusterization. Some of these oligomers might be already present in the pre-expansion chamber. Actually, dimers and other oligomers (up to tetramers) of methanol in vapor phase have been detected and quantified.[14] The kinematics of the expansion process, with only a small spread of atomic velocities, tends to favor this clustering mechanism by keeping gas molecules in the vicinity of each other. When the pressure in the jet is small, cluster growth mostly proceeds on the basis of monomer aggregation, basically leading to low mass clusters.

Besides, dimer formation is a three-body process, i.e., it needs the presence of a third body (the carrier gas) to stabilize the complex. So, Laval nozzles with gas mixtures of a condensable gas (like methanol) and a carrier gas are ideal settings for the formation of small clusters.

II.   *Formation of microdroplets by cluster aggregation*

Higher pressures in the jet or higher monomer concentrations, in turn, allow growth of clusters by aggregation or nucleation,[15] which leads to the production of large clusters or microdroplets.

Therefore the mass distribution of the clusters formed in a Laval nozzle strongly depends on the stagnation conditions (P_0 and T_0 and diameter of the nozzle throat) as well as on the condensable gas concentration.[13, 15]

Although neither SBGH (Ref. 4 of the manuscript) nor Gomez-Martin et al. (Ref. 8 of the manuscript) provide all details of their experiments, their stagnation pressures are lower than those used in the experiment of Laksmono et al. (Ref. 25 of the manuscript). Methanol concentration in the experiment of Gomez-Martin et al. ranges between 0.002-0.005% (with respect to the carrier gas), which is only slightly lower than the methanol concentration employed by Laksmono et al. (0.008-0.04%).

The Laval nozzle conditions in the Laksmono experiment are such that only monomers and microdroplets with average sizes ranging from 4.9 nm to 14.1 nm are observed at the nozzle exit.

As detailed below, in our opinion, the experimental conditions of Gomez-Martin et al. are such that one could observe the transition from oligomer formation to microdroplets. In particular, for methanol concentrations where k' depends linearly with [Met], only small oligomers are formed (via mechanism I). However, the downward curvature of k' vs [Met] plot is, in our opinion, a clear indication that bigger (and less reactive) clusters (microdroplets) are obtained. Actually, the deviation from linearity could be employed as a good measure for the onset of nucleation (*vide infra*).

In the following we provide a plausible explanation for the downward curvature of the k' vs [Met] plot obtained in the Laval nozzle experiments at the lowest temperatures. The reasoning is based on the fact that for small methanol concentrations only small oligomers exist, which are more reactive than the monomers as justified in our manuscript. By contrast, as [Met] increases bigger clusters form (as a consequence of nucleation of oligomers), which are less reactive than the dimer.

Linear dependence of k' on [Met]

Several theories have been employed to understand clusterization in supersonic expansions (like classical nucleation theory and other variants), but so far theory and experiments agree only qualitatively.

For a binary mixture of methanol monomers M and an oligomer of N units, methanol concentration can be expressed as:

$$[Met] = [M] + N[n - mer] \tag{S23}$$

If we assume that the oligomers are simply dimers D, then:

$$[Met] = [M] + 2[D] \tag{S24}$$

In the absence of an accurate theory capable of predicting the dependence of the molar fractions of monomer and dimer (x and $(1 - x)/2$, respectively) on the methanol concentration, we assume here that for small concentrations, the molar fractions remain constant. Figure 6 of ref [15] provides a hint that this might not be a bad assumption. The figure shows that the average oligomer size produced in a Laval nozzle expansion remains steady for low concentrations of the condensable gas (propane). Thus, the pseudo-first rate k' can be expressed as:

$$k'_{[Met]_{low}} = k_M[M] + k_D[D] = (k_M x + k_D(1 - x)/2)[Met] \tag{S25}$$

We have shown that $k_D \sim 100 k_M$ at $T = 50$ K. On the other hand, a fit of our calculations to the experimental results provides a value of ~ 0.7 for the molar fraction of the monomer x at 50 K. Therefore, for low methanol concentrations, the pseudo-first order rate depends linearly on [Met] as seen in the experiments:

$$k'_{[Met]_{low}} = 15.7 k_M[Met] \tag{S26}$$

Downward curvature of k' vs [Met]

As the methanol concentration increases there will be a point, called onset of nucleation,[15] where aggregation of small oligomers comes into play; this process leads to the formation of big clusters or micro-droplets (MD) (*vide supra*).

If we assume (for simplicity) that at high methanol concentrations, only monomers and micro-droplets of average size $< N >$ exist, then the pseudo first order rate reads:

$$k' = k_M[M] + k_{MD}[MD] \tag{S27}$$

which can be expressed as a function of monomer fraction:

$$k' = (k_M x + k_{MD}(1 - x)/< N >)[Met] \tag{S28}$$

Micro-droplet structures of methanol with 30-256 monomer units tend to achieve spherical-like shapes.[16] If the micro-droplet shape is approximated by a sphere, then, its radius r can be related to $< N >$ by:

$$r \propto \sqrt[3]{< N >} \tag{S29}$$

Since the OH + micro-droplet capture rate $k_{capt,MD}$ is proportional to r^2, we can express this rate as a function of cluster size as:

$$k_{capt,MD} \propto <N>^{2/3} \qquad (S30)$$

On the other hand, for micro-droplets the *substitution* mechanism, proposed for the dimers, does not obviously apply. Firstly because OH cannot easily replace a bulky cluster of $<N> - 1$ monomers, and secondly because the stability of the clusters increases with increasing cluster size until they attain a constant value.[17]

However, the big number of intermolecular vibrational modes of the micro-droplet provides an effective pathway for cooling, which ensures a longer lifetime of the OH$\cdots$MD cluster in comparison with the monomer. Overall, we can write the following equation $k_{MD} = Ck_M <N>^{2/3}$, where C is an unknown proportional constant. Therefore, the pseudo-first order rate reads:

$$k' = k_M \left(x + C \frac{(1-x)}{<N>^{\frac{1}{3}}} \right) [Met] \qquad (S31)$$

In the supersaturation region $<N>$ displays a linear dependence on the concentration of the condensable gas[15] ($<N> = C'[Met]$). Therefore:

$$k' = k_M \left(x[Met] + C''(1-x)[Met]^{2/3} \right) \qquad (S32)$$

Where $C'' = C/C'^{1/3}$ Assuming that $x = 0.7$ at $T = 50$ K, as for low [Met] and assuming a value of $C'' = 100$ (in concentration units$^{1/3}$) we obtain for the pseudo-first order rate at high methanol concentrations:

$$k'_{[Met]_{high}} = k_M \left(0.7[Met] + 30[Met]^{2/3} \right) \qquad (S33)$$

Figure S9 shows that the above equations (S26 and S33) can explain the downward curvature of k' observed in the experiments, and that these experiments could be employed to determine the onset of nucleation.
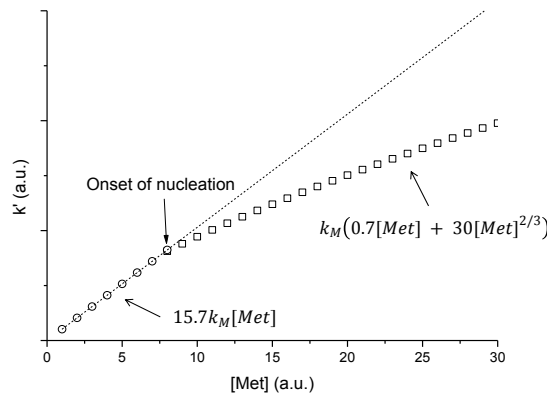
Figure S9. Predicted variation of the pseudo-first order rate coefficients as a function of methanol concentration in arbitrary units.

References

1.   Hess, W. P.; Tully, F. P., *J. Phys. Chem.* **1989,** *93* (5), 1944-1947.

2.   Meana-Pañeda, R.; Truhlar, D. G.; Fernandez-Ramos, A., *J. Chem. Phys.* **2011,** *134*, 094302.

3.   Gillespie, D. T., *J. Comput. Phys.* **1976,** *22*, 403-434.

4.   Rowley, R.; Tracy, C. M.; Pakkanen, T. A., *J. Chem. Phys.* **2006,** *125*, 154302.

5.   Hase, W. L.; Duchovic, R. J.; Hu, X.; Komornicki, A.; Lim, K. F.; Lu, D.-H.; Peslherbe, G. H.; Swamy, K. N.; Vande Linde, S. R.; Varandas, A.; Wang, H.; Wolf, R. J., *Quantum Chemistry Program Exchange (QCPE) Bulletin* **1996,** *16*, 671.

6.   Stimac, P.; Barker, J. R., *J. Phys. Chem. A* **2008,** *112*, 2553-2562.

7.   Shannon, R. J.; Blitz, M. A.; Goddard, A.; Heard, D. E., *Nat. Chem.* **2013,** *5*, 745-749.

8.   (a) Davies, J. W.; Green, N. J. B.; Pilling, M. J., *Chem. Phys. Let..* **1986,** *126*, 373-379; (b) Glowacki, D. R.; Lian, C.-H.; Morley, C.; Pilling, M. J.; Robertson, S. H., *J. Phys. Chem. A* **2012,** *116*, 9545-9560; (c) Fernandez-Ramos, A.; Ellingson, A.; Garret, B. C.; Truhlar, D. G., *Rev. Comput. Chem.* **2007,** *23*, 125.

9.   Gilbert, R. G.; Smith, S. C., *Theory of unimolecular and recombination reactions*. Blackwell Scientific Publications: Oxford, 1990.

10.   Jimenez, E.; Antinolo, M.; Ballesteros, B.; Canosa, A.; Albaladejo, J., *Phys. Chem. Chem. Phys.* **2016,** *18* (3), 2183-2191.

11.   Lewis, T. R.; Blitz, M. A.; Heard, D. E.; Seakins, P. W., *Phys. Chem. Chem. Phys.* **2015,** *17* (7), 4859-4863.

12.   (a) Kalikmanov, V. I., *Nucleation Theory*. Springer: Heidelberg, 2013; (b) Bergmann, D.; Ghosh, D.; Strey, R.; Wolk, J.; Tanimura, S.; Wyslouzil, B. E., *Homogenous Nucleation of a Homologous Serires of n-Alkanes in a Supersonic Nozzle*. Springer: 2007.

13.   Reinhard, P.-G.; Suraud, E., *Introduction to cluster dynamics*. Wiley: 2008.

14.   Renner, T. A.; Kucera, G. H.; Blander, M., *J. Chem. Phys.* **1977,** *66*, 177.

15.   Ferreiro, J. J.; Gartmann, T. E.; Schlappi, B.; Signorell, R., *Z. Phys. Chem.* **2015,** *229*, 1765.

16.   Wright, D.; El-Shall, M. S., *J. Chem. Phys.* **1996,** *105*, 11199.

17.   Boyd, S. L.; Boyd, R. J., *J. Chem. Theor. Comput.* **2007,** *3*, 54.